Comparative Analysis and Design of a Dual-Satellite System for Lunar Rover Localization

Kaila M. Y. Coimbra
Aeronautics and Astronautics
Stanford University
William F. Durand Building
496 Lomita Mall
Stanford, CA 94305
kcoimbra@stanford.edu

Grace Gao
Aeronautics and Astronautics
Stanford University
William F. Durand Building
496 Lomita Mall
Stanford, CA 94305
gracegao@stanford.edu

***Abstract*—The renewed international focus on lunar exploration has highlighted the need for autonomous localization services for lunar surface users. NASA's Endurance rover, tasked with traversing 2 000 km of the Moon's South Pole Aitken basin, is one such surface user that will require precise localization. The Lunar Pathfinder satellite is expected to maintain communication with the Endurance rover throughout its mission, enabling the possibility for satellite-based navigation. However, a key limitation of this approach is the poor observability and the lack of measurement diversity when relying on a single satellite. This paper presents a comparative analysis of the state estimation performance with the integration of a second communication satellite into the current planned configuration. We propose an optimized orbital design for the second satellite that maximizes coverage of the lunar South Pole region based on metrics such as line-of-sight visibility to the rover and position dilution of precision (PDOP). Additionally, we incorporate realistic error modeling that considers the receiver thermal noise, clock stability, and satellite ephemeris errors to best represent the scenario in simulation. The dual-satellite constellation design is able to localize the rover to sub-10-m accuracy in less than 1.11 hours on average, achieving a time reduction of 85.2% to 96.6% compared to the single-satellite scenario, depending on the rover's location. Note that this localization accuracy is achieved without a dedicated navigation payload onboard either satellite. These findings contribute to the development of more robust autonomous localization solutions for future lunar exploration.**

TABLE OF CONTENTS

1. INTRODUCTION

With the launch of the multi-mission NASA Artemis program, there is a growing need to develop autonomous localization services for lunar surface users. Vision-based navigation techniques, while useful, are often insufficient due to their high memory storage requirements and vulnerability to errors during the lunar night [1, 2]. Therefore, alternative methods must be considered to complement situations where vision-based navigation is less effective. Concurrently, multiple space agencies are developing LunaNet, a network of satellite networks designed to provide communication and navigation services to lunar surface users [3]. Early-stage missions, such as NASA's Endurance rover, will precede the full deployment of the LunaNet constellation [4]. Presently, one of LunaNet's initial pilot satellites, the Lunar Pathfinder, will provide communication-only services to the early-stage missions, including Endurance [5].

Establishing lunar positioning, navigation, and timing (PNT) services poses a significant challenge due to the limited infrastructure available in the cis-lunar environment. Previous works have proposed multi-satellite constellations designed to deliver navigation services to lunar users [6–8]. Other research has investigated the real-time positioning, velocity, and timing of a moving surface user using a minimal infrastructure consisting of a ground reference station and a three-satellite constellation [9]. This approach implements a joint Doppler and ranging technique to achieve sub-10-m accuracy. Despite these advancements, relying on multiple satellites and reference stations may not be feasible within the time frame of many early-stage missions, emphasizing the need for simpler and more easily deployable solutions.

In our prior work, we investigated the use of a single satellite to provide absolute localization to the Endurance rover [10, 11]. In this single-satellite scenario, the rover, while stationary, accumulates navigation observables from the satellite and refines its position estimation over time. One study assumes that the satellite has a radiometric navigation payload, which enables the use of two-way ranging measurements [10]. Conversely, the following study models the communication-only Lunar Pathfinder as the single satellite, necessitating the use of Doppler shift measurements from the downlinked communication signals as the only navigation observable [11]. However, the single-satellite localization method requires the rover to be stationary for up to 3.7 hours when using two-way ranging measurements [10], and up to 16.4 hours when using Doppler shift measurements to achieve the desired sub-10-m positioning accuracy [11], significantly limiting the operational capabilities of the rover.

In this work, we evaluate the localization performance of a surface user utilizing only a two-satellite constellation comprising of the Lunar Pathfinder and a second satellite with identical specifications. This represents the simplest deployable infrastructure beyond a single satellite, as neither satellite is equipped with a dedicated navigation payload, precluding the use of ranging measurements. Additionally, we do not rely on a lunar reference station to support localization in

979-8-3503-5597-0/25/$31.00 ©2025 IEEE

this study. The advantages of using a second satellite include an improved dilution of precision (DOP), faster convergence times in reducing the positioning errors, and better signal coverage of the lunar South Pole region. This paper quantifies the performance improvements achieved by adding a second communication satellite to the existing single-satellite architecture, which includes the Lunar Pathfinder. This analysis helps inform the decision on whether the additional costs of a second satellite are justified for localizing the Endurance rover.

Approach and Key Contributions

We first set up the simulation environment by modeling the antenna and states of the Lunar Pathfinder and the Endurance rover according to the specifications provided by the Surrey Satellite Technology Ltd. (SSTL) and ESA [5], as well as NASA [4]. We incorporate realistic error modeling to account for receiver thermal noise, clock stability, and ephemeris errors. Then, we conduct analyses on the geometric diversity and line-of-sight visibility of various orbits for the secondary, or auxiliary, satellite. Finally, we use a weighted batch filter to determine the time that it will take to localize the Endurance rover to the desired accuracy. For this study, we consider conservative ephemeris errors (4.48 m in position and 0.40 mm/s in velocity) to provide a direct comparison to the single-satellite scenario in [11] and also consider inflated ephemeris errors up to 100.00 m in position and 10.00 mm/s in velocity, which are more representative for communication satellites.

The key contributions of this work are as follows.

1) We investigate the absolute localization accuracy of a lunar surface user relying solely on two lunar satellites without dedicated navigation payloads.
2) We provide a direct comparison in the state estimation performance between a single-satellite and a dual-satellite scenario, with varying degrees of ephemeris errors.
3) We analyze various orbits to optimize the coverage of the lunar South Pole region using only a dual-satellite system.

Paper Organization

The paper is organized as follows: Section 2 describes how we model the Lunar Pathfinder and the auxiliary satellite, particularly the critical components for localization such as the orbit, communication signal, and transmitter antenna. Next, Section 3 provides details on how the Endurance rover is represented in simulation. Section 4 outlines the methodology for modeling measurement errors, including thermal noise, clock stability, and satellite ephemeris errors. In Section 5, we propose our state estimation framework. Finally, the experimental set-up and results of the study are detailed in Section 6 with concluding statements in Section 7.

2. DUAL-SATELLITE SYSTEM MODELING

We model the Lunar Pathfinder's orbit, communication signal, and transmitter antenna using the latest specifications released by SSTL and ESA [5]. In this study, we model the auxiliary satellite as an exact replica of the Lunar Pathfinder, which aligns with ESA's Moonlight scenario of eventually launching multiple Lunar Pathfinders [5]. Consequently, the communication signal of the auxiliary satellite is modeled identically to that of the Lunar Pathfinder.

Orbit Model

The Lunar Pathfinder follows an elliptical lunar frozen orbit (ELFO) with an orbital period of 10.84 hours. The orbital elements of the ELFO path are detailed in Table 1. Due to the Moon's rotation about its axis and the frozen nature of the Pathfinder's orbit, each revolution results in a slightly different coverage of the lunar surface. Every 28 days, the Moon completes a full revolution about its axis, and the Pathfinder's coverage of the lunar surface resets [4].

Table 1. **Lunar Pathfinder's orbital elements.**

Orbital Elements	Value
Semi-major axis [km]	5740
Eccentricity	0.58
Inclination [°]	54.856
RAAN [°]	0
Argument of the Periapsis [°]	86.322
Mean Anomaly [°]	180

For the auxiliary satellite, we also select an ELFO because of its stability and its ability to provide long-duration coverage of the South Pole region. In this work, we determine the mean anomaly and right ascension of the ascending node (RAAN) that maximizes the signal coverage of the dual-satellite system by conducting sensitivity studies of both elements independently. We constrain the auxiliary satellite's other orbital elements to be the same as those of the Lunar Pathfinder to maintain an elliptical frozen orbit. We consider mean anomalies from $-90°$ (equivalent to $270°$) to $90°$ and RAAN values from $30°$ to $240°$. The results of these sensitivity studies are detailed in Section 6.

Communication Signal Model

The Lunar Pathfinder provides S-band and Ultra-High Frequency (UHF) channels of communication to assets and uses X-band to relay data to Earth ground stations [5]. The Endurance rover will utilize the Lunar Pathfinder's S-band signals for communication [4]. The downlink frequency for S-band signals ranges from 2025 MHz to 2110 MHz, so we choose to use 2050 MHz for our simulations [5]. We assume that the communication signal employs convolutional encoding at a coding rate $r = 1/2$ with binary phase-shift keying (BPSK) modulation.

According to the Endurance specification document, the effective isotropic radiated power (EIRP) produced by the communication signal is 26.5 dB W [4]. This requirement is the maximum EIRP that the Lunar Pathfinder will transmit to an autonomous rover. We model the transmitter antenna gain pattern as having an EIRP of 26.5 dB W at boresight with a half-power beamwidth (HPBW) angle of $7.1°$, per the Lunar Pathfinder's specifications [5]. The off-boresight angle is calculated under the assumption that the satellite is always pointing in the nadir direction toward the center of the Moon. These communication signal parameters are summarized in Table 2.

Furthermore, we find that for autonomous rovers such as the Endurance rover, the mean contact time per day from the Lunar Pathfinder satellite is 529 minutes, or 8.82 hours [5]. Therefore, our aim is to localize the rover to the desired accuracy within this mean contact time per day metric.

Table 2. Communication signal parameters.

Parameters	Value
S-band downlink frequency f_C [MHz]	2050
Coding rate r	0.5
EIRP at boresight [dB W]	26.5
HPBW [°]	7.1

Satellite Clock

To the authors' knowledge, details about the clock selection for the Lunar Pathfinder satellite are not yet publicly available. For this study, we assume that the satellite will have a higher fidelity clock compared to the rover and that both the Lunar Pathfinder and the auxiliary satellite will use the Excelitas RAFS clock. Table 3 outlines the parameters of the Excelitas RAFS. Due to its stability, the h_{-1} and h_{-2} coefficients have a negligible contribution to the clock's Allan variance [12].

Table 3. Parameters for the Excelitas RAFS clock [12, 13].

Parameters	Value
Size [cm^3]	1645
Weight [kg]	6.35
Power [W]	39
TDEV per day [µs]	4.8×10^{-3}
h_0 [s^2/s]	8.0×10^{-27}
h_{-1} [s^2/s^2]	–
h_{-2} [s/s^2]	–

Doppler Shift Measurement Model

To localize the rover, we opportunistically extract Doppler shift observables from both satellites' communication signals to obtain pseudorange rate measurements. The Doppler shift observables are obtained by calculating the difference between the received frequency and the source frequency of the signal. From Doppler shift data, pseudorange rate measurements can be extracted as follows [14].

$$\dot{\rho} = -\frac{Dc}{f_C}, \tag{1}$$

where D is the observed Doppler shift, f_C is the signal's source frequency, and $c = 299\,792\,458$ m/s is the speed of light.

We simulate the Doppler shift data by modeling the pseudorange rate measurements that the rover will observe. We do so by augmenting the true pseudorange rate with clock drift and measurement errors.

$$\tilde{\dot{\rho}}(t) = \mathbf{v_s}(t) \cdot \frac{\mathbf{r_s}(t) - \mathbf{r_r}}{\|\mathbf{r_s}(t) - \mathbf{r_r}\|} + c\left(\dot{\delta t}_r - \dot{\delta t}_s\right) + \epsilon_{\dot{\rho}}, \tag{2}$$

where $\mathbf{r_r}$ is the true position of the rover, $\mathbf{r_s}$ and $\mathbf{v_s}$ are the true position and velocity of the satellite, and $\dot{\delta t}_r$ and d $\dot{\delta t}_s$ are the clock drifts of the rover and satellite, respectively. The measurement error term $\epsilon_{\dot{\rho}}$ is defined in Section 4 in (14). Note that the pseudorange rate equation does not include a clock bias term, as it is inherently removed by the time derivative.

3. ENDURANCE ROVER REPRESENTATION

In this section, we describe how the relevant details of the Endurance mission scenario are represented in simulation. We follow the Endurance rover's specification document [4] when applicable and outline any necessary assumptions below.

Rover Locations

In this work, we assume that the rover is stationary during the measurement accumulation window. We choose three waypoints along the rover's planned path as testing locations for our state estimation framework. The three locations–Apollo peak ring, Poincaré Q, and Artemis Basecamp–are labeled with their respective coordinates in Figure 1. These locations are chosen because they differ significantly in latitude and longitude with respect to each other and are a key waypoint for the Endurance mission.

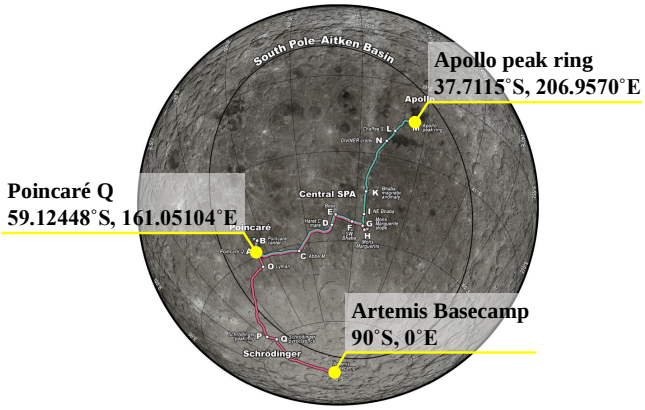

Figure 1. Chosen rover locations with labeled coordinates (figure adapted from [4]).

The rover's initial state estimate is sampled from a Gaussian normal distribution with a 3D standard deviation of 100 m, following the approach in [11]. A Gaussian distribution is chosen over a uniform distribution because we assume some prior knowledge, as the rover will be equipped with visual navigation capabilities [4]. This initial error is considered achievable through a combination of human-in-the-loop map matching upon landing and dead reckoning (aided by autonomous visual navigation) during traversal. While future work will constrain the initial error in the z direction, we maintain these larger error bounds in this work to enable direct comparison with prior work [11].

Rover Clock

The Endurance team has not yet released the type of clock that will be onboard the rover. In prior work, we conducted a sensitivity study where we evaluated the state estimation performance of the rover when the rover is equipped with clocks of various sizes, weights, and power consumptions (SWaP) [11]. The conclusion of the study is that the PRS 10 clock from the Stanford Research Systems (SRS) is a suitable clock for the use case of localizing the rover because of its minimal time deviation (TDEV) per day while also being low SWaP. Therefore, we assume the rover is equipped with the SRS PRS 10 clock for this work. The SWaP, TDEV per day, and power spectral density (PSD) coefficients used

to characterize the phase error of the rover's clock are listed in Table 4.

Table 4. **Parameters for the SRS PRS 10 clock [12, 13].**

Parameters	Value
Size [cm^3]	155
Weight [kg]	0.6
Power [W]	14.4
TDEV per day [µs]	7.0×10^{-2}
h_0 [s^2/s]	1.3×10^{-22}
h_{-1} [$\mathrm{s}^2/\mathrm{s}^2$]	2.3×10^{-26}
h_{-2} [s/s^2]	3.3×10^{-31}

Receiver Antenna Model

The Lunar Pathfinder will be the Endurance rover's only source of communication, as direct-to-Earth communication will not be feasible given the rover's location on the far side of the Moon. The Endurance rover will be equipped with a 75-cm high-gain omnidirectional antenna to receive S-band frequencies at a gain of 22.5 dBi. The antenna will track the Lunar Pathfinder with a margin of 3°, which results in a gain loss of only 0.5 dB [4]. Thus, we model the receiver antenna gain G_r to be 22 dB.

The rover will also be equipped with a redundant low-gain antenna at 3 dBi for emergency scenarios [4]. In this study, we assume that the high-gain antenna will be fully operational throughout the rover's mission.

Carrier-to-Noise Density Ratio C/N_0 Model

The received carrier-to-noise density ratio C/N_0 describes the quality of the signal when it has reached the rover's antenna. We require the signal strength to be larger than 30 dB Hz for the rover to acquire Doppler shift observables (this requirement is also set in other literature such as [15]). We model C/N_0 using the following equation, as is done in our prior work [10, 11].

$$C/N_0 = P_r + g/T - k \tag{3}$$

The received isometric power P_r is a function of EIRP and the free space path loss. EIRP is dependent on the off-boresight angle β, which is discussed in Section 2. The gain-to-noise-temperature ratio g/T of the receiver is a function of the receiver gain G_r and the equivalent noise temperature T_{eq}. The final term in (3) is the Boltzmann constant $k = -228.6$ dB W/(K Hz). More details on the C/N_0 modeling can be found in [10, 11].

4. ERROR MODELING

If the auxiliary satellite is equipped with a communication payload, both the auxiliary satellite and the Lunar Pathfinder will be subject to one-way Doppler measurements errors. According to the Deep Space Network specifications [16], the three main contributions to the measurement error are thermal noise at the receiver, phase noise in the frequency source and local oscillators, and phase scintillation when passing through the solar corona. Given that we are modeling one-way Doppler measurements between a lunar surface user and satellites in an ELFO, we can assume that the error contribution due to phase scintillation is negligible.

Thermal Noise

In [16], the downlink thermal noise contribution σ_t^2 is modeled as

$$\sigma_t^2 = \frac{2B_L}{C/N_0 \cdot S_L}\left(\frac{c}{2\pi f_C T}\right)^2, \tag{4}$$

where B_L is the bandwidth of the downlink carrier loop, C/N_0 is the received carrier-to-noise density ratio, f_C is the downlink carrier frequency, T is the integration time, and c is the speed of light. The squaring loss of the Costas loop S_L is represented as

$$S_L = \frac{2E_S/N_0}{1 + 2E_S/N_0}, \tag{5}$$

$$\frac{E_S}{N_0} = \frac{E_b}{N_0} r b_{sym}, \tag{6}$$

where E_S/N_0 is the telemetry symbol energy to noise spectral density ratio and E_b/N_0 is the energy per bit to noise power spectral density (PSD) ratio [16–18]. The coding rate r is $1/2$ when using a convolutional code for the downlink S-band communication signal [5]. Furthermore, we assume that the Lunar Pathfinder uses a BPSK modulation, which transfers 1 bit per symbol ($b_{sym} = 1$). Using a bit error rate (BER) of 1×10^{-6}, the E_b/N_0 is approximately 10.5 dB for BPSK [19]. We include a margin of an additional 3 dB to this required E_b/N_0 value. These parameters, summarized in Table 5, result in a thermal noise error σ_t on the order of 10^{-1} mm/s during strong signal strength. When the received carrier-to-noise density ratio C/N_0 rapidly decreases as the satellite approaches occlusion, the thermal noise error σ_t can spike to an order of 10^1 mm/s.

Table 5. **Parameters for thermal noise [5, 16–19].**

Parameters	Value
Bandwidth B_L [Hz]	1
Integration time T [s]	0.02
Energy per bit to noise PSD ratio E_b/N_0 [dB]	13.5
Bit per symbol b_{sym}	1

Clock Stability

To model the phase error σ_c^2, we make the following approximation.

$$\sigma_c^2 \simeq c^2\left(\sigma_{c,s}^2 + \sigma_{c,r}^2\right), \tag{7}$$

where $\sigma_{c,s}$ and $\sigma_{c,r}$ are the Allan deviations of the satellite's and rover's clocks, respectively [16]. The phase error is modeled as a random walk with covariance $\mathbf{Q}$. Given that we are finding the noise in the clock drift, we only need to account for the variance in the fractional frequency, or Allan variance q_{22} [20]. Note that the Allan variance is dependent

on the measurement sampling time τ.

$$\mathbf{Q} = \begin{bmatrix} q_{11} & q_{12} \\ q_{21} & q_{22} \end{bmatrix}, \tag{8}$$

$$q_{11} = \frac{\tau}{2} h_0 + 2\tau^2 h_{-1} + \frac{2\pi^2 \tau^3}{3} h_{-2}, \tag{9}$$

$$q_{12} = q_{21} = \tau h_{-1} + \pi^2 \tau^2 h_{-2}, \tag{10}$$

$$q_{22} = \frac{1}{2\tau} h_0 + 4h_{-1} + \frac{8\pi^2 \tau}{3} h_{-2} \tag{11}$$

The PSD coefficients h_0, h_{-1}, and h_{-2} are specific to the type of clock and described in Table 3 and 4. Using these parameters, the phase deviation σ_c becomes $1.8\ \mathrm{mm/s}$.

Satellite Ephemeris Errors

For the satellites' ephemeris errors, we reference the Lunar Communications Relay and Navigation Systems (LCRNS) specifications in their Lunar Relay Services Requirements Document (SRD). In the SRD, they cite that the 3σ signal-in-space errors (SISE) for 1-way forward Doppler reference signals of a lunar relay PNT satellite will be $13.43\ \mathrm{m}$ in position and $1.2\ \mathrm{mm/s}$ in velocity (averaged over a $10\ \mathrm{s}$ integration period) [21]. The SISE contributions include errors due to the satellite's knowledge of its own state, the integrity of the transmitted signal, and the transmitting ephemeris and clock data to the ground users. Thus, we assume that the satellites' clock errors are encapsulated by the SISE contributions.

In Section 6, we also consider inflated ephemeris errors for both satellites to better represent the expected ephemeris errors for communication satellites. Table 6 lists the position and velocity ephemeris errors at 1σ that we consider in this study. We use the ephemeris errors in the LCRNS specifications for most of the analyses unless otherwise specified.

Table 6. Ephemeris errors at 1σ that are considered in this study.

Type	Position $\sigma_{e,p}$ [m]	Velocity $\sigma_{e,v}$ [mm/s]
LCRNS	4.48	0.40
Inflated	100.00	10.00

When the rover predicts its expected measurements for the filtering process, the rover has erroneous knowledge of the satellite's position $\tilde{\mathbf{r}}_{\boldsymbol{s}}$ and velocity $\tilde{\mathbf{v}}_{\boldsymbol{s}}$. We incorporate these ephemeris errors in position $\epsilon_{e,p}$ and velocity $\epsilon_{e,v}$ (using standard deviations defined in Table 6) into the predicted measurements as such:

$$\tilde{\mathbf{r}}_{\boldsymbol{s}} = \mathbf{r}_{\boldsymbol{s}} + \epsilon_{e,p} \quad , \quad \epsilon_{e,p} \sim \mathcal{N}(0, \sigma^2_{e,p_{xyz}} \mathbf{I}_{\mathbf{3}\times\mathbf{3}}) \tag{12}$$

$$\tilde{\mathbf{v}}_{\boldsymbol{s}} = \mathbf{v}_{\boldsymbol{s}} + \epsilon_{e,v} \quad , \quad \epsilon_{e,v} \sim \mathcal{N}(0, \sigma^2_{e,v_{xyz}} \mathbf{I}_{\mathbf{3}\times\mathbf{3}}) \tag{13}$$

We model the ephemeris errors as Gaussian noise rather than in terms of bias and drift for several reasons: (1) there is currently limited information on the expected bias and drift for the ephemeris of lunar satellites, as the schedule and availability of Earth ground station support have not yet been determined. (2) The timing and frequency at which the rover will receive updated ephemeris information from the satellite, which are currently unknown, directly affect the rover's state estimation performance. A Gaussian noise model avoids the need to rely on specific assumptions about update intervals. (3) While a bias-and-drift model would result in smaller errors on average by capturing the gradual accumulation of errors over time, a Gaussian noise model ensures that ephemeris errors are not underestimated throughout the measurement window, which is critical for informing the design of a dual-satellite system. In summary, given the lack of well-characterized metrics, a Gaussian noise model provides a sufficient and robust representation of ephemeris errors for this study.

Measurement Errors

The measurements observed by the rover are affected by white thermal noise at the receiver and phase noise from the frequency sources. The clock drifts from the rover and the satellite are included in the pseudorange rate model in (2). As previously noted, the clock bias term is intentionally excluded in the model through differentiation. Therefore, the measurement error term for one-way Doppler measurements for each satellite is as follows.

$$\epsilon_{\dot{\rho}} \sim \mathcal{N}(0, \sigma^2_{\dot{\rho}}) \quad , \quad \sigma^2_{\dot{\rho}} = \sigma^2_t + \sigma^2_c \tag{14}$$

For the scenario in which both satellites employ Doppler shift measurements, we describe the total measurement error as the sum of contributions from the satellite's ephemeris errors and the predicted measurement errors.

$$\sigma^2_{tot} = \sigma^2_{e,v} + \sigma^2_{\dot{\rho}} \tag{15}$$

This metric places a higher weight for low-variance measurements during the filtering process.

5. State Estimation Framework

We design a weighted batch filter framework to refine the rover's state estimate from the observed pseudorange rate measurements and the rover's noisy knowledge of the satellite's state. We choose to use a weighted batch filter over other frameworks such as an Extended Kalman Filter (EKF) because it retains the history of all previous measurements, which is useful for a low-observable system such as our scenario. Future work will investigate the state estimation performance using filtering methods that update based on the information at a single time step.

State Formulation

We define the rover's position $\mathbf{r}_{\boldsymbol{r}}$ to be the 3D position, as detailed in (16). The rover's state $\mathbf{x}_{\boldsymbol{r}}$, which includes clock drift, is defined in (17). We do not need to account for clock bias in the rover's state because we only consider pseudorange rate measurements in the filter.

$$\mathbf{r}_{\boldsymbol{r},k} = \begin{bmatrix} x_k & y_k & z_k \end{bmatrix}^\top, \tag{16}$$

$$\mathbf{x}_{\boldsymbol{r},k} = \begin{bmatrix} \mathbf{r}_{\boldsymbol{r},k} & c \cdot \dot{\delta} t_{r,k} \end{bmatrix}^\top \tag{17}$$

In this formulation, k is the number of iterations of the batch filter required for the Euclidean norm of $\delta \mathbf{x}_k$ to be less than a small tolerance ϵ_{tol}.

$$\delta \mathbf{x}_k = \hat{\mathbf{x}}_{\boldsymbol{r},k+1} - \hat{\mathbf{x}}_{\boldsymbol{r},k} \tag{18}$$

Filter Formulation

The filter outputs a new state estimate after a batch of N measurements have been accumulated per satellite. We assume that the measurement sampling rate is the same for both satellites. The measurement vector $\tilde{\mathbf{y}}$ stacks the N observed pseudorange rates from the first and second satellites.

$$\tilde{\mathbf{y}} = \begin{bmatrix} \tilde{\dot{\rho}}_1(t_1) & \dots & \tilde{\dot{\rho}}_1(t_N) & \tilde{\dot{\rho}}_2(t_1) & \dots & \tilde{\dot{\rho}}_2(t_N) \end{bmatrix}^\top \quad (19)$$

As mentioned in Section 3, the rover's initial position estimate $\hat{\mathbf{r}}_{\boldsymbol{r}}(0)$ is sampled using a Gaussian normal distribution with zero clock drift. With each iteration k of the filter, we update the expected rover's state estimate $\hat{\mathbf{x}}_{\boldsymbol{r},k}$ by minimizing the weighted Euclidean norm of the difference between the observed and the next expected pseudorange rate measurements, as shown below.

$$C = \|\tilde{\mathbf{y}} - \hat{\mathbf{y}}_{k+1}\|^2_{\mathbf{W}}\,, \quad (20)$$

where $\hat{\mathbf{y}}_{k+1}$ is the stack of next expected pseudorange rate measurements, which has a similar form to (19). We show a concatenated matrix of $\hat{\mathbf{y}}_{k+1}$ in (21). Note that $\mathbf{W}$ is the weighting matrix as defined later in this section. The expected pseudorange rate at the next iteration $k+1$ at any given time t is a function of the next expected rover's position estimate $\hat{\mathbf{r}}_{\boldsymbol{r},k+1}$, the next expected rover's clock drift estimate $\hat{\delta t}_{r,k+1}$, and the rover's noisy knowledge of the satellite's current position $\tilde{\mathbf{r}}_{\boldsymbol{s}}(t)$ and velocity $\tilde{\mathbf{v}}_{\boldsymbol{s}}(t)$. The satellite's expected clock drift $\hat{\dot{\delta t}}_s$ is a constant value obtained from the time deviation of the clock. The formulation to obtain the expected pseudorange rate at iteration $k+1$ is detailed in (22).

$$\hat{\mathbf{y}}_{k+1} = \begin{bmatrix} \hat{\dot{\rho}}_{1,k+1}(t_1) & \dots & \hat{\dot{\rho}}_{2,k+1}(t_N) \end{bmatrix}^\top \quad (21)$$

$$\hat{\dot{\rho}}_{k+1}(t) = \tilde{\mathbf{v}}_{\boldsymbol{s}}(t) \cdot \frac{\tilde{\mathbf{r}}_{\boldsymbol{s}}(t) - \hat{\mathbf{r}}_{\boldsymbol{r},k+1}}{\|\tilde{\mathbf{r}}_{\boldsymbol{s}}(t) - \hat{\mathbf{r}}_{\boldsymbol{r},k+1}\|} + c\left(\hat{\delta t}_{r,k+1} - \hat{\dot{\delta t}}_s\right) \quad (22)$$

By performing a first-order Taylor approximation of $\hat{\mathbf{y}}_{k+1}$, we can obtain a solution $\delta\mathbf{x}_k$ of the cost function in (20) [22].

$$\delta\mathbf{x}_k = \left(\mathbf{J}_k^\top \mathbf{W} \mathbf{J}_k\right)^{-1} \mathbf{J}_k^\top \mathbf{W} \delta\mathbf{y}_k\,, \quad (23)$$

where $\delta\mathbf{y}_k$ is the measurement residual, $\mathbf{W}$ is the weighting matrix, and the Jacobian matrix $\mathbf{J}_k$ is the first-order derivative of the expected pseudorange rates $\hat{\mathbf{y}}_k$ with respect to the state estimate $\hat{\mathbf{x}}_{\boldsymbol{r},k}$.

Due to the noise introduced into the system, we are incentivized to place a higher weight on measurements with less variance through a weighting matrix $\mathbf{W}$. We filter the measurements using the total measurement error for each satellite as defined in (15), resulting in a square matrix of size $(2t_N \times 2t_N)$.

$$\mathbf{W} = \mathrm{diag}\left(\boldsymbol{\sigma}_{\boldsymbol{tot,1}}^{\boldsymbol{-2}}\,,\ \boldsymbol{\sigma}_{\boldsymbol{tot,2}}^{\boldsymbol{-2}}\right) \quad (24)$$

Weighted PDOP Formulation

Within the state estimation framework, we also store the weighted position dilution of precision (PDOP) values over time. $PDOP_{\mathbf{W}}$ is the square root of the trace of the weighted covariance matrix $\mathbf{M}$. We only consider the diagonal elements of $\mathbf{M}$ that correspond to the 3D position (x, y, z).

$$\mathbf{M} = (\mathbf{J}_k^\top \mathbf{W} \mathbf{J}_k)^{-1} \quad (25)$$

$$PDOP_{\mathbf{W}} = \sqrt{M_{11} + M_{22} + M_{33}} \quad (26)$$

We use the weighted PDOP to determine which orbits for the auxiliary satellite result in the best measurement diversity for localizing the Endurance rover.

6. Experimental Set-Up and Results

In this section, we discuss how we set up the simulation environment and the performance metrics used for our analyses. We conduct sensitivity studies to determine the optimal orbital elements for the auxiliary satellite that minimizes PDOP, while still maintaining an elliptical frozen orbit. Then, we discuss the results of the state estimation performance under the dual-satellite system. Finally, we compare the conclusions of the study conducted in this paper to the findings of the single-satellite scenario [11].

Simulation Parameters

Starting at an initial epoch of October 1, 2030 00:00:00 UTC, we run the simulation over two orbital periods of the Lunar Pathfinder, which amounts to 21.68 hours. Since the rover's initial state estimate is randomly sampled, we average the state estimation performance across 100 Monte Carlo realizations. The simulation parameters are summarized in Table 7.

The measurement sampling rate is set to 0.5 Hz, and the filter updates every 180 seconds. These values are chosen to have sufficient granularity in measurements and results when evaluating the rover's state estimation performance. While fine-tuning these parameters could further enhance the operational performance, sensitivity analyses of the sampling and update rates are beyond the scope of this study.

Table 7. Simulation parameters.

Parameters	Value
Measurement sampling rate [Hz]	0.5
Filter update interval [s]	180
Total simulation length [hr]	21.68
Batch filter tolerance ϵ_{tol}	10^{-9}
Number of Monte Carlo runs	100

Auxiliary Satellite Orbit Selection

We conduct sensitivity analyses on the mean anomaly M_0 and RAAN Ω of the orbit to determine the optimal orbit for the auxiliary satellite. We conduct a search over these two orbital elements and constrain the remaining four elements to ensure that the orbit is elliptical and frozen. Intuitively, a diametrically opposed orbit to the Lunar Pathfinder ($M_0 = 0°$, $\Omega = 180°$) is expected to maximize the geometric diversity of the constellation. To evaluate this intuition, we first fix $M_0 = 0°$ and analyze the weighted PDOP of the dual-satellite system as a function of RAAN. The analysis identifies the RAAN that best minimizes the mean weighted PDOP across the three selected rover locations. PDOP is preferred over HDOP because we do not constrain the rover's z position in this study.

Using the RAAN that produces the lowest weighted PDOP, we fine-tune the mean anomaly for the auxiliary satellite that maximizes the total time that at least one satellite is visible to the rover. Visibility is selected as the performance metric for the mean anomaly study because the mean anomaly determines the satellite's position along its orbit, directly impacting the satellite's visibility duration. In contrast, weighted PDOP better reflects geometric diversity, which is less sensitive to changes in mean anomaly.

While this approach decouples the sensitivity studies for mean anomaly and RAAN, future work will extend the analysis to include a two-dimensional search over both orbital elements to optimize the constellation design more holistically.

Weighted PDOP Analysis with Varying RAAN Ω

Using a fixed mean anomaly of $M_0 = 0°$, we conduct a weighted PDOP analysis to determine which RAAN Ω for the auxiliary satellite results in the best measurement diversity. In this study, we consider Ω values from $30°$ to $240°$ for the auxiliary satellite. Figure 2 shows the weighted PDOP for the dual-satellite constellation in blue-yellow-green colors and the single-satellite system (Lunar Pathfinder only) in red. The weighted PDOP with two satellites is one to two orders of magnitude lower in comparison to the single-satellite scenario, as desired. The Ω value that corresponds to the lowest weighted PDOP differs for each location. For lower-latitude regions such as the Apollo peak ring and Poincaré Q, Ω values of $150°$ to $210°$ result in the best satellite geometry for measurement diversity. However, we find that even higher Ω values of $240°$ also have low weighted PDOP values for regions in the lunar South Pole, such as the Artemis Basecamp.

To determine the optimal Ω value for the auxiliary satellite across all three locations, we evaluate the mean weighted PDOP for RAAN values at $10°$ intervals. The RAAN value that corresponds to the smallest mean weighted PDOP throughout the entire measurement window is $200°$ for the Apollo peak ring, $140°$ for Poincaré Q, and $90°$ for the Artemis Basecamp, as listed in Table 8. Based solely on these values, a RAAN value of approximately $140°$ appears to offer the best compromise for all three locations. However, as shown in Figure 2, the weighted PDOP varies significantly throughout the measurement window. To prevent early PDOP values from disproportionately influencing the total mean, the measurement window is divided into three equal segments–0 to 7 hours, 7 to 14 hours, and 14 to 21 hours–and the mean is calculated for each segment. Figure 3 presents the mean weighted PDOP over these 7-hour intervals for each rover location.

Table 8. The RAAN value that corresponds to the lowest mean weighted PDOP for the entire measurement window and for each 7-hour segment.

Location	Time interval			
	All	0-7 hrs	7-14 hrs	14-21 hrs
APR	200°	200°	180°	180°
PQ	140°	140°	150°	150°
AB	90°	90°	160°	170°

As expected, the first interval from 0 to 7 hours exhibits the highest variability and the largest values of mean weighted PDOP. In fact, the weighted PDOP values from the first 7-hour interval dominates the mean over the entire measurement window, resulting in the same optimal RAAN values, as seen in Table 8. To better account for the lowest weighted PDOP observed later in the measurement window, we assign equal weight to the means from each segment and each location. This approach yields an optimal RAAN value of approximately $160°$.

Visibility Analysis with Varying Mean Anomaly M_0

After optimizing the RAAN Ω to $160°$, we perform a sensitivity study on the mean anomaly to determine what the optimal offset for the auxiliary satellite's initial position relative to the Lunar Pathfinder's initial position at $M_0 = 180°$. This analysis aims to maximize the percentage of time at least one satellite is visible to the rover at any given location. Satellite visibility is defined as satisfying both of the following criteria: the elevation mask must be greater than $5°$ and the carrier-to-noise density ratio C/N_0 must be greater than 30 dB Hz. Figure 4 shows the percentage of time during which at least one satellite is visible to the rover over a simulation period of two orbital periods, or 21.68 hours. The study evaluates mean anomalies for the auxiliary satellite ranging from $-90°$ (equivalent to $270°$) to $90°$.

Since the Artemis Basecamp is located at the Moon's South

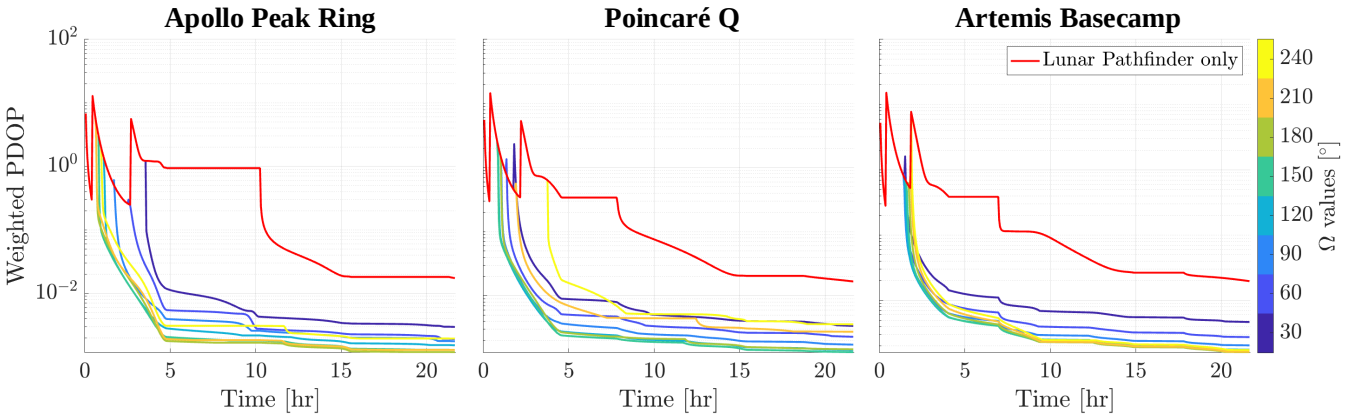

Figure 2. Weighted PDOP for the dual-satellite system with varying RAAN Ω for the auxiliary satellite. The weighted PDOP for the single-satellite system (Lunar Pathfinder only) is shown in red.

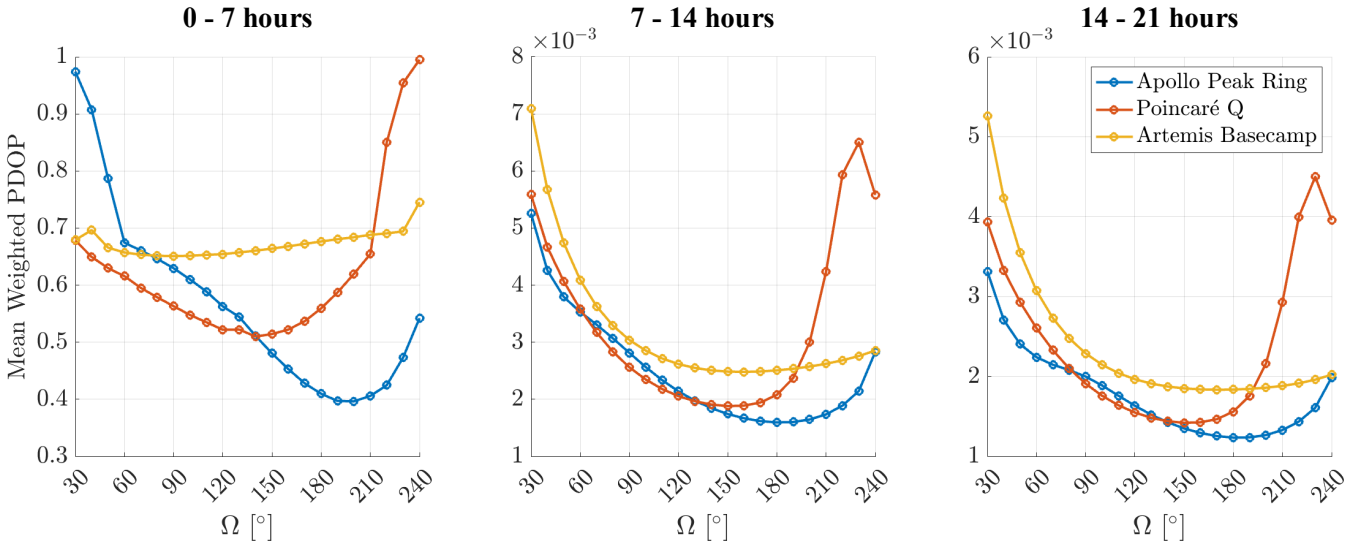

Figure 3. Mean weighted PDOP over 7-hour intervals as a function of the auxiliary satellite's RAAN.

Pole, the percentage of time during which at least one satellite is visible is symmetric about $M_0 = 0°$. However, for lower latitudes, the satellites' occultation zones overlap at $M_0 = 0°$, resulting in intervals where no satellite is visible to the rover. To avoid these visibility gaps, placing the auxiliary satellite at mean anomalies of $M_0 = -70°$ and $-80°$ relative to the Lunar Pathfinder's mean anomaly of $M_0 = 180°$ ensures continuous visibility throughout the simulation for all selected locations. In this study, we select a mean anomaly of $M_0 = -70°$ (equivalent to 290°) for the auxiliary satellite, which corresponds to a 250° mean anomaly offset relative to the Lunar Pathfinder.

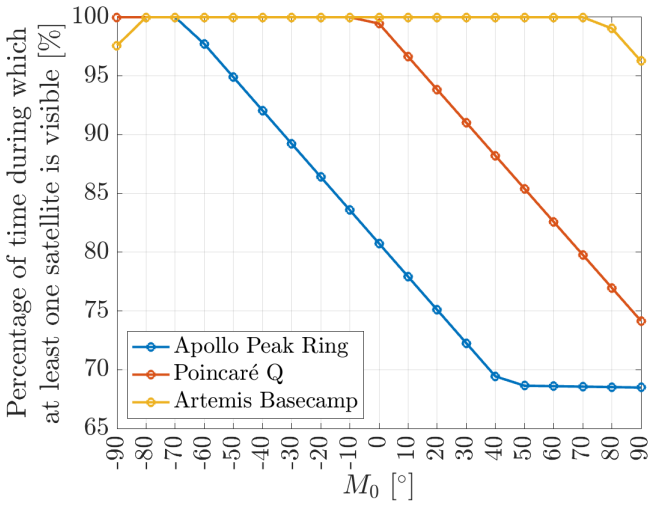

Figure 4. Percentage of time during which at least one satellite is visible to the rover, evaluated for auxiliary satellite mean anomaly values from $-90°$ (equivalent to 270°) to 90°.

State Estimation Performance

Through our weighted PDOP analysis and visibility study, we select an orbit with mean anomaly $M_0 = -70°$ (equivalently, 290°) and RAAN $\Omega = 160°$ for the auxiliary satellite. The other orbital elements for the auxiliary satellite are equivalent to that of the Lunar Pathfinder to maintain an elliptical frozen orbit and are described in Table 1.

The orbital paths of the dual-satellite system are shown in Figure 5. The red segments of the paths indicate when each satellite is visible when the rover is located at the Artemis Basecamp. The gray zones are when the satellites are behind the Moon with respect to the rover.

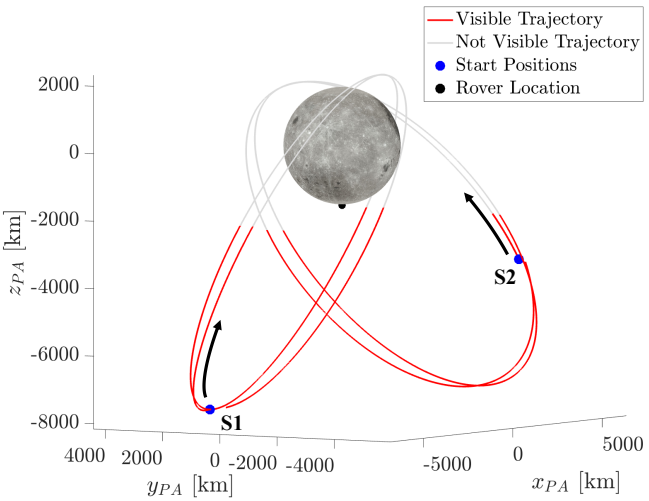

Figure 5. The orbital paths of the dual-satellite system, where Lunar Pathfinder is S1 and the auxiliary satellite is S2. The occultation zones in gray correspond to when the rover is located at the Artemis Basecamp.

For the selected orbital paths, the received carrier-to-noise density ratio C/N_0 maintains its strength above the 30 dB Hz threshold, until the satellites are occluded by the Moon. Recall that a satellite is considered occluded when its elevation angle drops below 5°. Figure 6 shows the received C/N_0 by the Lunar Pathfinder (Satellite 1) and the auxiliary satellite

(Satellite 2) when the rover is located at the Artemis Basecamp.

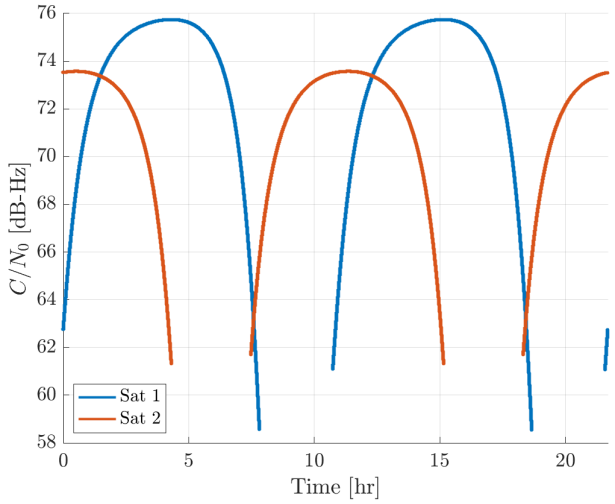

Figure 6. The received carrier-to-noise density ratio C/N_0 when the rover is located at the Artemis Basecamp.

With the completed auxiliary satellite's orbit design, we can now investigate the state estimation performance of the rover using the dual-satellite system. As described in Section 5, we use a weighted batch filter to refine the rover's position and clock drift over time. Figure 7 shows the positioning error over time when the rover is located at the Artemis Basecamp. Note that the measurement accumulation for the filtering begins when both satellites are in view (this assumption also applies for Figure 8). The blue and red lines denote the mean μ and 99 percentile across 100 Monte Carlo realizations and the light blue shaded regions indicate the 1σ bounds. The light gray area is the occultation period of the Lunar Pathfinder (Satellite 1) and the darker gray area is the occultation period of the auxiliary satellite (Satellite 2). For the state estimation results, the performance metric is the time it takes for the mean and 99 percentile across 100 Monte

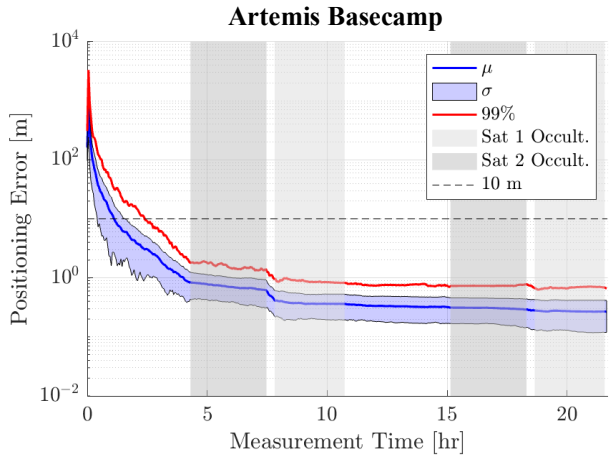

Figure 7. The positioning error of the rover over time when located at the Artemis Basecamp. The filter is not initialized with the rover's initial state estimate.

Carlo runs to achieve a positioning error of less than 10 m. When located at the Artemis Basecamp, the rover achieves a localization accuracy of sub-10-m within 1.12 hours, on average, and 2.39 hours at the 99 percentile.

As shown in Figure 7, the current filtering formulation introduces an initial spike in positioning error. This spike can be eliminated without compromising long-term performance by augmenting the measurement vector $\delta\mathbf{y}_k$ with the rover's initial position estimate. Consequently, the Jacobian matrix $\mathbf{J}_k$ is expanded with $[\mathbf{I_{3\times3}}, \mathbf{0_{3\times1}}]$ and the weighting matrix $\mathbf{W}$ is updated to include the rover's initial positioning error. This initialization technique is applied, and the resulting state estimations are shown in Figure 8 for the rover at the Apollo peak ring, Poincaré Q, and the Artemis Basecamp.

Overall, we find that the dual-satellite system is able to localize the Endurance rover to the desired accuracy in less than 1.11 hours, on average, for all locations. We find that even the 99 percentile was able to localize well within the mean contact time per day for the Lunar Pathfinder, which is 8.82 hours. The times for the mean and 99 percentile to reach sub-10-m in the dual-satellite system are summarized in Table 9. The Artemis Basecamp has the slowest convergence in comparison to the other locations, which is as expected since the Artemis Basecamp location resulted in the largest weighted PDOP values for $\Omega = 160°$ (see Figure 3). Even so, the Artemis Basecamp location still achieved the desired localization accuracy within less than an hour of the other locations' convergence time.

Comparison to the Single-Satellite Scenario

In our prior work investigating the localization performance of the single-satellite scenario, we find that the Lunar Pathfinder was able to localize the rover to the desired accuracy within 7.5 to 11.6 hours, on average. Using similar modeling methods for clock and ephemeris errors, we find that the dual-satellite system is able to decrease the mean localization time by 96.6%, 97.2%, and 85.2% for the Apollo peak ring, the Poincaré Q, and the Artemis Basecamp, respectively. Table 9 summarizes the localization times when using a one-satellite scenario (the Lunar Pathfinder only) and when using a two-satellite scenario (the Lunar Pathfinder and the auxiliary satellite).

Table 9. The time, in hours, to localize the rover at the desired accuracy of less than 10 m at each key waypoint for one- and two-satellite scenarios. Results for the one-satellite scenario are obtained from [11].

No. of Sat.	Location	Time to reach $\leq$ 10 m	
		Mean [hr]	99 percentile [hr]
1	APR	11.5	14.4
	PQ	11.6	16.0
	AB	7.5	16.4
2	APR	0.39	0.73
	PQ	0.33	0.65
	AB	1.11	2.39

For the state estimation performances thus far, we have assumed that both satellites have ephemeris errors according to the LCRNS specifications [21] detailed in Section 4. Since precise ephemeris knowledge is more critical to the function of navigation satellites in comparison to communication satellites, the requirements on ephemeris errors are

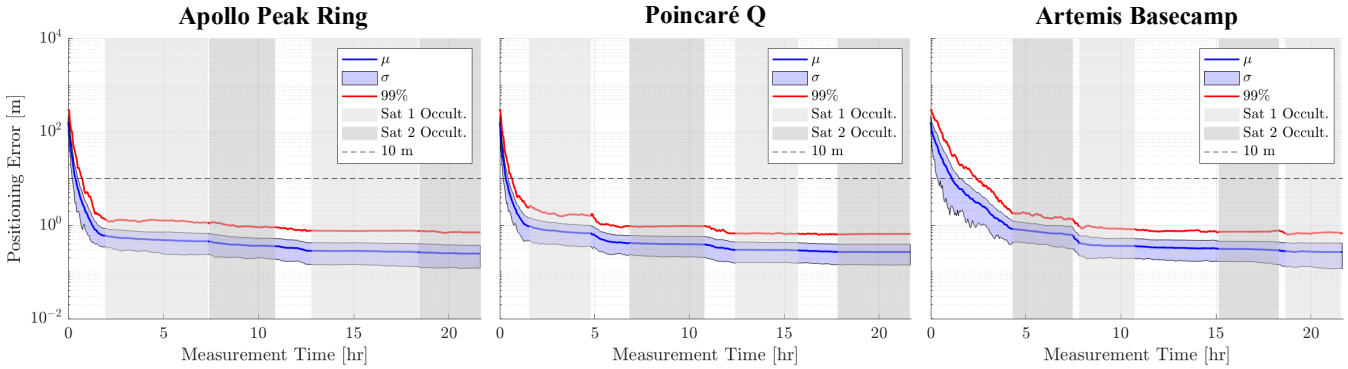

Figure 8. **The positioning error of the rover over time for all three waypoints. The measurement vector is augmented with the rover's initial position estimate.**

likely to be looser for communication satellites. Therefore, we also investigate the state estimation performance with inflated ephemeris errors for both communication satellites in the system. Table 10 shows the mean and 99 percentile localization times with ephemeris errors of 100.00 m in position and 10.00 mm/s in velocity. We find that the dual-satellite system with ephemeris errors that are two orders of magnitude worse than that of the single-satellite scenario is still able to localize several hours faster. Thus, we conclude that the localization time and accuracy of the Endurance rover will improve significantly with the addition of a second communication satellite.

Table 10. **The time, in hours, to localize the rover at the desired accuracy of less than 10 m at each key waypoint when both satellites are afflicted with ephemeris errors of 100.00 m in position and 10.00 mm/s in velocity.**

Location	Time to reach $\leq$ 10 m	
	Mean [hr]	99 percentile [hr]
Apollo Peak Ring	1.05	2.25
Poincaré Q	1.04	4.02
Artemis Basecamp	2.56	7.51

7. CONCLUSIONS

In this work, we present a two-satellite constellation design that is well-suited in localizing the Endurance rover in the South Pole Aitken basin of the Moon. We use a weighted batch filter framework that accumulates Doppler shift measurements from two communication satellites and refines the rover's state estimate over time. Using conservative estimates of the satellites' ephemeris errors, our framework was able to achieve the desired sub-10 m localization accuracy in under 1.11 hours for all key waypoints considered in this study. The dual-satellite system decreased the state estimation time by 85.2% to 96.6%, depending on the rover's location, when comparing to the single-satellite system. We also conduct sensitivity analyses on the second satellite's orbital elements to determine which orbits result in the best signal coverage of the lunar South Pole region.

In summary, this work offers key insights into enhancing navigation capabilities for early-stage missions with limited access to multiple lunar satellites. Additionally, this work demonstrates that accurate surface localization is achievable on the Moon using satellites without dedicated navigation payloads. Extensions of this work will compare the convergence time when the auxiliary satellite is equipped with a navigation payload capable of transmitting ranging measurements to surface users. Future studies will also investigate the achievable localization performance when the rover is able to communicate with lunar ground stations.

ACKNOWLEDGMENTS

This work is supported by the Stanford Knight-Hennessy Scholars graduate fellowship and the NSF Graduate Research Fellowship No. DGE-2146755. We would like to thank Keidai Iiyama for reviewing this paper. We would also like to acknowledge the Stanford Navigation and Autonomous Vehicles (NAV) Laboratory for their helpful feedback.

REFERENCES

[1] S. Daftry, Z. Chen, Y. Cheng, S. Tepsuporn, S. Khattak, and L. Matthies, "LunarNav: Crater-based Localization for Long-range Autonomous Lunar Rover Navigation," *2023 IEEE Aerospace Conference*, 2023.

[2] A. Cauligi, R. M. Swan, H. Ono, S. Daftry, J. Elliot, L. Matthies, and D. Atha, "ShadowNav: Crater-Based Localization for Nighttime and Permanently Shadowed Region Lunar Navigation," *2023 IEEE Aerospace Conference*, 2023.

[3] NASA and ESA, "Lunanet interoperability specification document, draft version 5," https://www.nasa.gov/directorates/somd/space-communications-navigation-program/lunanet-interoperability-specification/, NASA and ESA, Tech. Rep., Aug 2023.

[4] J. T. Keane, S. M. Tikoo, and J. Elliot, "Endurance: Lunar South Pole-Aitken Basin Traverse and Sample Return Rover," *NASA Jet Propulsion Laboratory, Technical Report*, 2022. [Online]. Available: https://tinyurl.com/2p88fx4f

[5] SSTL, "Lunar Pathfinder: Data relay satellite in orbit around the Moon," *SSTL, Service Guide (V4)*, 2022. [Online]. Available: https://www.sstl.co.uk/getmedia/9efe3cc5-6b5b-

4fd1-bbd7-443bc2d21848/Lunar-Pathfinder-Service-Guide-V004.pdf

[6] M. Leonardi, G. Sirbu, C. Stallo, M. Eleuteri, C. Di Lauro, C. Iannone, and E. Del Zoppo, "Autonomous Lunar Satellite Navigation System: Preliminary Performance Assessment on South Pole," *Proceedings of the 2021 International Technical Meeting of The Institute of Navigation*, pp. 478–490, January 2021. [Online]. Available: https://doi.org/10.33012/2021.17843

[7] M. Murata, I. Kawano, and S. Kogure, "Lunar Navigation Satellite System and Positioning Accuracy Evaluation," *Proceedings of the 2022 International Technical Meeting of The Institute of Navigation*, pp. 582–586, January 2022. [Online]. Available: https://doi.org/10.33012/2022.18220

[8] A. D. Arcia Gil, D. Renwick, C. Cappelletti, and P. Blunt, "Methodology for optimizing a constellation of a lunar global navigation system with a multi-objective optimization algorithm," *Acta Astronautica*, vol. 204, pp. 348–357, 2023. [Online]. Available: https://www.sciencedirect.com/science/article/pii/S009457652300005X

[9] W. W. Jun, K.-M. Cheung, and E. G. Lightsey, "Improved Surface Positioning with Measurement Differences in Joint Doppler and Ranging," *2023 IEEE Aerospace Conference*, 2023.

[10] M. Cortinovis, T. Mina, and G. Gao, "Assessment of Single Satellite-based Lunar Positioning for the NASA Endurance Mission," *2024 IEEE Aerospace Conference*, pp. 1–11, 2024.

[11] K. M. Y. Coimbra, M. Cortinovis, T. Mina, and G. Gao, "Single-Satellite Lunar Navigation via Doppler Shift Observables for the NASA Endurance Mission," *Proceedings of the Institute of Navigation GNSS+ conference (ION GNSS+ 2024)*, 2024.

[12] B. L. Schmittberger and D. R. Scherer, "A Review of Contemporary Atomic Frequency Standards," *arXiv preprint arXiv:2004.09987*, 2020.

[13] S. Bhamidipati, T. Mina, and G. Gao, "A Case Study Analysis for Designing a Lunar Navigation Satellite System with Time-Transfer from Earth-GPS," *Proceedings of the Institute of Navigation ITM conference (ION ITM 2022)*, 2022.

[14] P. Misra and P. Enge, *Global Positioning System: Signals, Measurements & Performance*. Ganga-Jamuna Press, 2012.

[15] F. T. Melman, P. Zoccarato, C. Orgel, R. Swinden, P. Giordano, and J. Ventura-Traveset, "LCNS Positioning of a Lunar Surface Rover Using a DEM-Based Altitude Constraint," *Remote Sensing*, vol. 14, no. 16, p. 3942, 2022.

[16] A. O'Dea, P. Kinman, T. T. Pham, and C. Chang, "Doppler tracking," *Deep Space Network, DSN No. 810-005, 202, Rev. C*, 2019.

[17] W. Damm, "Signal-to-Noise, Carrier-to-Noise, EbNo on Signal Quality Ratios," *Webinar with Maury Microwave*, 2010. [Online]. Available: https://www.noisecom.com/Portals/0/webinars/SN%20CN%20EbNo.pdf

[18] D. Forney, "Principles of Digital Communication II," *MIT OpenCourseWare*, 2005. [Online]. Available: https://ocw.mit.edu/courses/6-451-principles-of-digital-communication-ii-spring-2005/resources/mit6_451s05_fulllecnotes/

[19] C. Heegard and S. B. Wicker, *Turbo coding*. Kluwer Academic Publishers, 1999.

[20] T. Krawinkel and S. Schön, "Benefits of receiver clock modeling in code-based GNSS navigation," *GPS Solutions*, vol. 20, pp. 687–701, 2016. [Online]. Available: https://doi.org/10.1007/s10291-015-0480-2

[21] NASA, "Lunar communications relay and navigation systems (LCRNS)," *Preliminary Lunar Relay Services Requirements Document (SRD)*, 2022.

[22] B. D. Tapley, B. E. Schutz, and G. H. Born, *Statistical Orbit Determination*. Elsevier, 2004.

BIOGRAPHY

Kaila M. Y. Coimbra *received her B.S. in Mechanical Engineering, with a minor in Aerospace Engineering, from the California Institute of Technology in 2023. She is currently a Ph.D. student in the Department of Aeronautics and Astronautics at Stanford University. Her research interests include positioning, navigation, and timing, particularly for lunar surface rovers.*

Grace Gao *is an Associate Professor in the Department of Aeronautics and Astronautics at Stanford University. Before joining Stanford University, she was an assistant professor at the University of Illinois Urbana-Champaign. She obtained her Ph.D. degree at Stanford University. Her research is on robust and secure positioning, navigation, and timing with applications to manned and unmanned aerial vehicles, autonomous driving cars, as well as space robotics.*